

A study of nonlinear processes in space plasmas

Abstract. In this article, readers are invited to explore the world of computational simulations of space plasmas. The computational experiment is similar to the traditional laboratory experiment. Neither can it, nor will it be able to solve all the physical problems that remain poorly understood, but it does provide a powerful tool to help physicists (scientists) seek solutions for them. We show first that when the Courant-Friedrich-Lewy or CFL condition is not met, numerical instability occurs. We also present simulations of electrostatic solitary waves (ESWs). We note that ESWs can be generated as a result of the nonlinear coalescence of strong electrostatic waves excited by electrostatic beam instability. This instability is caused by the drift of a beam of electrons relative to ions and other electrons drifting with the ions. The ion thermal velocity must be high enough to prevent the decay of electrostatic waves to ion acoustic waves, a prerequisite for the production of ESWs. Another condition is that the drift density of the electron beam with respect to the ions must be 30% greater than plasma density.

Streszczenie. W artykule przedstawiono symulację plazmy kosmicznej. Tradycyjny eksperyment obliczeniowy nie może, ani nie będzie w stanie rozwiązać wszystkich problemów fizycznych, które pozostają słabo poznane, ale zapewnia narzędzie pomagające fizykom w poszukiwaniu ich rozwiązania. Najpierw pokazujemy, że gdy warunek Couranta-Friedricha-Lewy'ego lub CFL nie jest spełniony, występuje niestabilność numeryczna. Przedstawiamy symulacje elektrostacyjnych pojedynczych fal (ESW). Zauważamy, że ESW mogą być generowane w wyniku nieliniowej koalescencji silnych fal elektrostacyjnych wzbudzanych przez niestabilność wiązki elektrostacyjnej. Ta niestabilność jest spowodowana dryfowaniem wiązki elektronów względem jonów i innych elektronów dryfujących wraz z jonami. (Badanie procesów nieliniowych w plazmach kosmicznych)

Keywords: Space plasmas, computer simulation, PIC codes, ESW solitary waves

Słowa kluczowe: plazma kosmiczna, zjawiska nieliniowe, model Couranta-Friedricha-Lewy'ego

1. Introduction

Traditionally, the scientific method involves mutual interpretation between laboratory experiments and theories. In the laboratory, experiments are made several times in a controlled way, allowing the scientist to observe the behavior of the system and the most appropriate physical description to explain the phenomenon under study. For several years, theories have been successfully developed in this way. In recent decades, with advances in technology, another type of experimentation has been devised to help scientists model the complex form of phenomena that govern the laws of nature.

The computational experiment helped bridge the gap between theory and laboratory experiments. The basic idea of a computational experiment is to simulate in a controlled way the physical behavior of a complex system by solving a set of mathematical equations based on a fundamental physical-mathematical model well accepted by the scientific community.

Although similar to traditional laboratory techniques in which the physical parameters have been changed in a controlled way, computational experiments provide certain advantages in helping obtain detailed information about the system: Diagnoses are non-invasive, i.e. they do not disrupt the system. Physical effects may or may not be taken into consideration, making it possible to identify which is the most important causative agent for an observed phenomenon and, above all, the experiments can be reproduced in the same way, without being impacted by external agents. They also have the advantage of allowing the study of linear, non-linear and time-dependent phenomena. Usually, in traditional experiments, obtaining diagnoses disrupts the system under study.

The wider the gap between theory and design, the greater the benefits of computational design. In space, experiments are conducted through satellite observations, active experiments in space, and active and passive measurements of the Earth. Gaining information from these experiments is very costly and time consuming. Due to the complexity of the phenomena that occur in space plasmas and the difficulty of obtaining on-site information, often only in one single region of space, the results of these

observations can lead to misinterpretation and non-understanding of the phenomenon. In some cases, computational experiments can globally reproduce certain phenomena that could not be treated analytically or experimentally.

The complex nature of the problems encountered in space plasma Physics has triggered the interest in and the devising of codes for the development of space theories on plasma. In addition, numerical simulations also contribute in the development of high performance computer systems and behavioral predictions of new plasma physics equipment and experiments, such as controlled thermonuclear fusion reactors (Tokamak) and others. Traditionally, the study of complex physical phenomena relies on two complementary approaches: the theoretical approach and the experimental approach, two very powerful techniques with however significant intrinsic limitations. Great advances in physics have come from the combination of these two approaches.

The experimental approach consists in observing the behavior of the physical environment that we wish to study after having disrupted it in a controlled way. This method turns out to be difficult in the case of very large-scale physical phenomena (space plasmas) where observations are limited to measuring the response of the environment to uncontrolled and most often unknown disturbances. The measurement points obtained are punctual and do not yield a precise and full representation of certain phenomena.

The theoretical approach is based on the use of analytical techniques to determine the behavior of a system. This approach uses simplifying assumptions:

- Limited number of parameters;
- Symmetry research;
- Use of a simple theory in the form of linear expansions and / or series expansions.

Important advances in Physics have originated from the combination of these two approaches. However, the success of these approaches must be tempered due to the existence of systems for which experimentation is difficult and which consist of a large number of degrees of freedom whose analytical treatment is unpractical.

As most of the interesting natural physical phenomena

correspond to this category, we opted to study them through numerical simulation.

This method is based on the postulate that the physical laws used describe reality and can be formulated mathematically. These characteristics are summarized as follows:

- Modeling of the theory or the environment to be validated;
- Use of basic principles;
- Full control of system parameters;
- Taking into account all phenomena, be they linear or non-linear.

Numerical simulation is therefore a very powerful analytical tool, but it is only justified as a bridge between theory and experimental observation.

Computational plasma simulation includes two broad areas of activity, one based on kinetic description and the other on the description of fluids.

A. Fluid description

In the fluid description [1, 2], we are interested in the evolution of plasma volumes, small when compared to the size of the system but containing a very high number of particles (see Fig.1). The observables are macroscopic mechanical and electrodynamic quantities (averaged over small volumes, density, charge density, overall speed, temperature, kinetic energy density, current, etc.) whose evolution is followed. This type of simulation makes it possible to reproduce large-scale phenomena. This approach has inherent limitations, among which:

- The introduction of transport coefficients;
- The obligation to follow Maxwellian functions.

B. Kinetic description

description [2], we directly take into account the fundamental forces acting on each particle (gravitation, Lorentz force, etc.). This approach is carried out either by numerically solving the Vlasov or Fokker-Planck equations (see Fig. 1), or by particle simulations which calculate the motion of a large number of particles interacting with one other and with electromagnetic fields. This description is used when the distribution function deviates from the Maxwellian distribution (wave-particle interaction, shock waves). Using the basic principles allows the study all aspects, whether linear or non-linear. This approach seems the simplest and the most complete but it encounters implementation problems which limit the scope of its validity.

There are so-called hybrid simulations [3, 4] which take into account the advantages of both descriptions, fluid (large-scale phenomena: electrons and cold electrons) and kinetic (microscopic phenomena), by treating certain components of the plasma as fluid while others are processed kinetically. Such an approach requires the introduction of phenomenological parameters that can introduce distortions in the physical results obtained.

C. Use of a particle code

Among the existing numerical models, the simplest from a conceptual point of view remains the particle code. In this type of model, we match each type of physical plasma particle to a simulated particle in the computer's memory and all the interaction forces acting on each particle are calculated. Although this method appears to be easy, in practice it turns out to be complex due to the limitations of computing resources. Physically, ions and electrons are treated in most cases as point charges. Some reactions between these particles develop over short distances in short intervals of time. The most important effects are long-range interactions or collective effects which occur over

much larger scales of time and space. The collective effects only take into account the interaction of a very large number of particles. To this effect, the concept of macro-particles has been introduced. Since computer resources do not allow all physical particles to be tracked individually, it is common to use digital particles known as super particles each having a statistical weight to represent a set of particles.

The PIC (Particle-in-cell) method is considered to be the first method to have been developed historically for the simulation of Vlasov Maxwell or Vlasov Poisson equations.

This method consists in coupling a particle method for Vlasov and a mesh method for Poisson or Maxwell. The principle of the method is to discretize the distribution function by a set of macro-particles representing at the initial moment a realization of the law of probability associated with the initial distribution function. These macro-particles are advanced in time by numerically solving their equation of motion in an electromagnetic field. Coupling with the field solver is done by calculating the sources, charge and current densities for Maxwell's equations using a regularization method. A classic field solver can be used. To continue the loop in time, the fields at the positions of the particles (Fig.2) must be calculated. The literature on this method is abundant [3, 5-7].

D. Kinetic simulation model

Kinetic simulations have been successfully applied in the treatment of basic physical problems in which the particle distribution function deviates considerably from the Maxwell distribution under stochastic heating, particle trapping or wave-particle resonance [2]. MHD simulations are generally applied to large-scale problems, directly related to the behavior of experimental devices or, for example, to the simulation of the global and dynamic structure of the magnetosphere on a large scale. In general, kinetic simulation models (like the one used in our work) follow the diagram shown in Fig.3), where we first determine the type of simulation and the approximations to be included in the model, the type of system under study (whether electrostatic or electromagnetic), geometry, initial conditions and boundary conditions. These last three are very important, as they will include all the physical conditions of the system under study, such as the region in which the system is located and the characteristics of that region. After having correctly determined the numerical model which best represents the physical system under study, the kinetic particle simulations use the solutions of Maxwell's equations, based on self-coherent sources (density and plasma currents) [4], generated by the position and velocity of the charged particles representing the plasma subjected to electromagnetic fields. During simulations, it is necessary to take into account the external fields and the fields generated by the movement of the charged particles themselves. Often, this process involves advancing the particles over a short period, or no time, Δt , to collect the source terms used to calculate the fields.

Once the new fields have been obtained, the particles can be moved again so that the source terms are updated and the process is repeated as many times as necessary. Basic scheme is (Fig.3). First step is to read the initial conditions, particle positions x_i and velocities v_i represented by sub index $i = 1, 2, 3 \dots N_{total}$, where N_{total} is the maximum particle-size number of the system because calculation of charge density in mesh grid point depends on distance of particle from that point.

In second step, some weighting has to be done because calculation of charge density in mesh grid depends on distance of distance of particle from that point.

Fluid Code (MHD, Multi Fluid)	
$\rho(x, t)$	Eulerian variables
$B(x, t)$	
$v(x, t)$	

Hybrid Code	
Ions	Particles
Electrons	Fluid
Hot electrons	Particles
Cold electrons	Fluid

Particle Code	
$x(t), v(t)$	Lagrangian variables
$E(x, t), B(x, t),$ $J(x, t)$	Eulerian variables

Vlasov Code	
$f(x, v, t)$	Particle distribution function
$E(x, t), B(x, t),$ $J(x, t)$	Eulerian variables

Fig.1. Classification of simulation codes

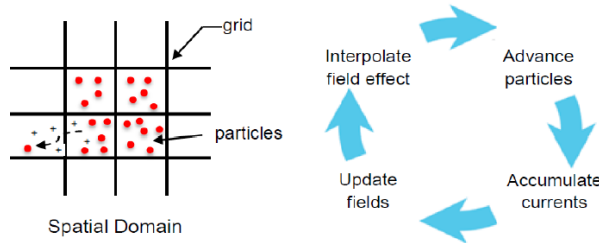


Fig.2. Principle of Particle In Cell (PIC) method

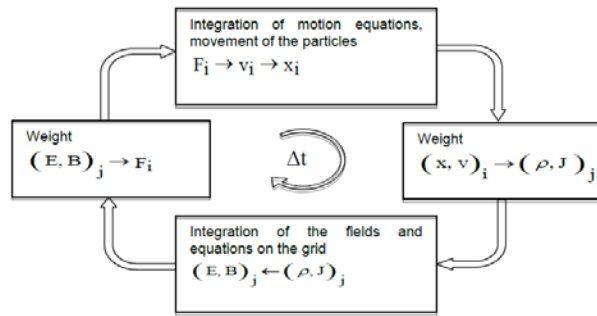


Fig.3. Typical cycle of a time step in a simulation program, the particles are numbered by $i = 1, 2, 3, \dots, N_{total}$; the grid indices are indicated by j which represent vectors in 2 and 3 dimensions [3].

After obtaining charge densities we proceed with integration of field equations. The fields are obtained only in the spatial grid, discrete points of space represented by sub index $j = 1, 2, 3 \dots P_{total}$ where P_{total} is the number of points of the spatial grid. Next, we weight how the field in individual grid point affects each particle. From the velocity and position of the particles, the charge and current densities in the spatial grid are calculated using a weighting function to calculate the electric and magnetic fields. The force used to move the particles is obtained by interpolation from the grid, again through the weighting function. The last step is integration of equation of motion and to accordingly

change position and velocity of particles. This cycle is repeated throughout the simulation [2-8]. The simulation follows step by step Δt , using the numerical method which guarantees sufficient stability and numerical precision. The time-step should be small compared to the wave period under study, $w_p \Delta t \ll 1$, where w_p is the local frequency of the plasma. The time-step must be small enough to allow the observation of the variations of the phenomena under study. Usually, fields are calculated in the spatial grid from charge and current density. Accuracy requires that the grid spacing, Δx for one-dimensional simulation, be small compared to the shortest wavelength of interest / worth considering, $k \Delta x \ll 1$. Using an inadequate temporal and spatial grid may introduce false physical behavior in the system, minimized by choosing appropriate parameters for the simulation [2].

2. Lagrangian formalism or Particle-in-Cell theory

2.1. Basic equations

The most natural way to follow the (\vec{x}, \vec{v}) phase-space evolution of a plasma is to consider the evolution of each particle over time. In the absence of collisions, the trajectory equations are reduced to the following two equations:

$$(1) \quad \frac{d\vec{x}}{dt} = \vec{v}$$

$$(2) \quad \frac{d\vec{v}}{dt} = \vec{a}$$

The Lorentz force \vec{F}_L for a particle of mass m and charge q in an electromagnetic field (\vec{E}, \vec{B}) is written:

$$(3) \quad \vec{F}_L = q(\vec{E} + \vec{v} \wedge \vec{B})$$

Knowledge of the forces acting on the particles as well as of the impact of the initial conditions (\vec{x}_0, \vec{v}_0) entirely defines the trajectory of the particles over time. For a particle of mass m and charge q , the equation (2) is written as follows:

$$(4) \quad m \frac{d\vec{v}}{dt} = q(\vec{E} + \vec{v} \wedge \vec{B})$$

Where electric field E and magnetic field B have been introduced. Electric and magnetic fields are defined by the Maxwell equations given below :

$$(5) \quad \vec{\nabla} \cdot \vec{E} = \frac{\rho}{\epsilon_0}$$

$$(6) \quad \vec{\nabla} \cdot \vec{B} = 0$$

$$(7) \quad \vec{\nabla} \wedge \vec{E} = -\frac{\partial \vec{B}}{\partial t}$$

$$(8) \quad \vec{\nabla} \wedge \vec{B} = \mu_0 \vec{J} + \mu_0 \epsilon_0 \frac{\partial \vec{E}}{\partial t}$$

Coupling occurs between the positions of the particles on the one hand and the electric field that is itself coupled with the magnetic field on the other.

$J \equiv (J_x, J_y, J_z)$, ρ , c , ϵ_0 and μ_0 are the current density, charge density, light speed, electric permittivity and magnetic permittivity respectively. ϵ_0 and μ_0 satisfy the relation:

$$(9) \quad \epsilon_0 \mu_0 = \frac{1}{c^2}$$

2.2. One-dimensional electrostatic model

Motion of computer particles is determined in two steps. From initial currents and charge densities we calculate electromagnetic field by using Maxwell' equations. Then we use this field in Newton equation to move particles for a small distance accordingly. Then we recalculate the fields from new particle positions and charge density. We are repeating these two steps during all simulation and simulate particle movement in mean field surrounding them. Rather than to solve equations of motion and Maxwellian equations in continuous space and time, we divide the physical volume into cells by lines which run parallel to the boundaries. The intersections of these lines define set of points called mesh points or grid points (particle in cell simulation). In these points we calculate the charge fields and relative to these points, we move our particles. Their space coordinates are continuous and then can occupy position anywhere within the mesh.

2.3. Space-time discretization

As mentioned previously, several methods have been developed to allow the numerical resolution of differential equations describing a physical system [9]. One of the most widely used methods to discretize differential equations is finite difference [9]. A good approximation for calculating the first derivative, df/dx , and the second derivative, d^2f/dx^2 , of a function f varying continuously over an interval Δx can be obtained from equations (10) and (11) using the finite difference method.

$$(10) \quad \frac{df}{dx} = \frac{f_{j+1} - f_{j-1}}{2\Delta x}$$

$$(11) \quad \frac{d^2f}{dx^2} = \frac{f_{j+1} - 2f_j + f_{j-1}}{\Delta x^2}$$

Figures (4) and (5) show the geometric diagram to obtain derivatives by using the finite difference method. In particle simulation, space and time must be discretized. The spatial discretization is introduced for two reasons. The first reason is due to the way the force acting on the particles is calculated [8], because instead of calculating the total contribution of the Coulomb force of all the particles, the force acting on a super particles is calculated by the field quantities defined at adjacent grid points. The second reason is that the super particles has a finite size over a certain region of space, so a spatial resolution less than the size of the super particles is unnecessary and meaningless [10]. Normally, the spatial grid spacing varies from one to three Debye lengths; this value has been obtained through numerical experiments [11, 12]. Numerical stability is directly related to this factor. If a spacing greater than three Debye lengths is chosen, numerical instability appears [8] and, therefore, the simulation results will have no physical significance. Another important factor is the number of particles per point in the grid. The higher the number of particles per point in the grid, the weaker the numerical fluctuations linked to the calculation of the electromagnetic fields. A more detailed study on numerical instability can be found in [13] and [14]. Temporal discretization is an inevitable technique in any numerical approximation to solve partial differential equations. A question that always arises is what value to assign to the time step. The answer will be: always as small as possible. The choice of this value must be such that there is numerical stability during the simulation. A condition which avoids numerical instability and which is generally used in computer simulation is the Courant-Friedrich-Lewy (CFL) condition given by:

$$(12) \quad \Delta x > v_{\max} \Delta t$$

where Δx is the spatial step, Δt is the time step and v_{\max} the maximum velocity that the particles of the system can acquire. This condition guarantees that, in a time step, the distance traveled by the particles of velocity v_{\max} must not be greater than Δx .

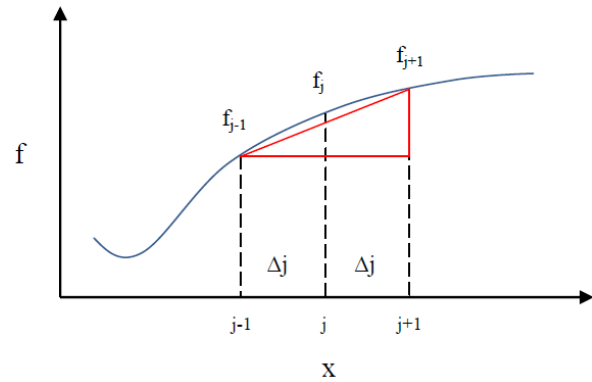


Fig.4 . Approximation for the first derivative of a function f

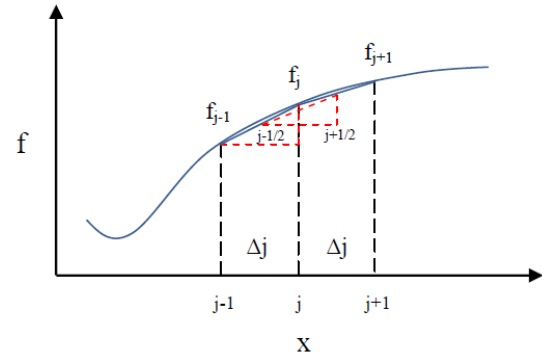


Fig.5. Approximation for the second derivative of a function f

For example, this condition can be obtained by the propagation of an electromagnetic wave in vacuum, the dispersion ratio of which is given by $\omega^2 = k^2 c^2$, where ω is the frequency of the wave, k the number of waves and c the speed of light in vacuum. Assuming that this electromagnetic wave can be represented by $A(x, t) = A_0 \exp[i(kx - \omega t)]$ where $A(x, t)$ is the amplitude of the wave at time t and A_0 is the amplitude at time $t = 0$, using the finite difference method centered in space and time, the derivative of $A(x, t)$ with respect to x will be given by:

$$(13) \quad \begin{aligned} \frac{\Delta A}{\Delta x} &= \frac{A(x_0 + \Delta x/2, t) - A(x_0 - \Delta x/2, t)}{\Delta x} \\ &= \frac{\exp(ik\Delta x/2) - \exp(-ik\Delta x/2)}{\Delta x} A(x_0, t) \\ &= i \frac{\sin(k\Delta x/2)}{\Delta x/2} A(x_0, t) \end{aligned}$$

By comparing $\Delta A / \Delta x$ to the partial spatial derivative $\partial A / \partial x$, we can see that the wave number k can be replaced by K represented by:

$$(14) \quad K = \frac{\sin(k\Delta x/2)}{\Delta x/2}$$

In the same way, the frequency ω can be replaced by a frequency Ω given by:

$$(15) \quad \Omega = \frac{\sin(\omega\Delta t/2)}{\Delta t/2}$$

By substituting Ω and K in the dispersion relation of the previous electromagnetic wave, we get:

$$(16) \quad \Omega^2 = c^2 K^2$$

For the highest wavelength $k_{\max} = \pi / \Delta x$ we will have:

$$(17) \quad \sin^2(\omega \Delta t / 2) = \left(\frac{c \Delta t}{\Delta x} \right)^2$$

If $c \Delta t / \Delta x > 1$, ω becomes complex, generating numerical instability, if $c \Delta t / \Delta x = 1$, the system will be slightly stable and if $c \Delta t / \Delta x < 1$, the system will be stable so that no numerical instability will be introduced. This is the standard CFL condition [12].

A geometric example of the CFL condition can be seen in figure (7). In case (a), the continuous curve represented by $\Delta x / \Delta t = v = c$, where v is the speed of propagation of information in the system, the CFL condition is found on the dotted curve which characterizes speed c , while maintaining the system at a stable level. For case (b), the curve $\Delta x / \Delta t = v > c$ will make the system numerically unstable, which means that the information will propagate at a speed greater than c . In case (c), $\Delta x / \Delta t = v < c$, the system becomes stable, so that the information propagates at a speed lower than c .

In [15], a detailed treatment of the numerical solutions of hyperbolic equations can be obtained.

2.4. Super particles

It can be said that the particle simulation method consists of following the movement of a large number of particles under the action of forces produced by the movement of the particles themselves, due to the interaction between them and / or externally applied fields. In general, the region of interest contains an extremely high number of particles. For example, in the interplanetary medium (region near the sun), the typical particle density of plasma is in the range of 10^4 to 10^6 m^{-3} . From a direct estimation, we can see that this number of particles is not plausible on most current computers, since the number of arithmetic operations on particles is quite high and hence the time required to solve the forces involved in the system by step integration would be too large, making simulations impractical.

To work around this problem, the concept of super particles was introduced. It is a mathematical model representing many particles of real plasma of finite size, with their charge distributed over a finite region of space [12].

Super particles were originally introduced by two research groups to provide statistical fluctuations and short-range collisions caused by a delta function [16-19, 20]. In other words, for point particles, in numerical terms, the potential tends towards infinity when the radius of the particle tends towards zero.

Several methods have been developed to determine the charge and current densities of super particles at points on the spatial grid.

One of the area-weighting methods developed was the nearest grid point, the nearest grid point (NPG), which equally weights all particles within a certain distance of the considered grid point [19]. Other grid load weighting schemes are called Cloud In Cell (CIC) or Particle In Cell (PIC).

These two methods have a slight difference: in the CIC method, the position of the particle determines its center while for PIC; the particle is limited by the positions of the closest grid points, regardless of their position in the cell [11].

Super particles can take any shape and the fundamental difference between them is how they accumulate charges at points on the grid based on their positions. However, the most commonly used super particles in simulations are called square (1), triangular (2) and Gaussian (3) [10-12], as shown in figure (6).

Since the super particle is idealized to represent many particles of a real plasma, the charge density, mass and energy of the super-particles must be the same as that of real particles [12], that is to say:

$$\text{Densité de charge} \rightarrow N_s Q_s = N_r Q_r;$$

$$\text{Densité de masse} \rightarrow N_s M_s = N_r M_r;$$

$$\text{Densité d'énergie} \rightarrow N_s k_B T_s = N_r k_B T_r.$$

The subscripts s and r denote the super particles and the real particle, respectively. N , Q , M , k_B and T are digital density, charge, mass, Boltzmann constant and temperature, respectively.

These parameters ensure that all basic physical parameters remain the same for real particles and super particles during the simulation. For example, charge-to-mass ratio, plasma frequency, cyclotron frequency, thermal velocity, and Debye length, $\lambda_D = v_{\text{the}} / \omega_{pe}$ where ω_{pe} is the electronic frequency of the plasma and v_{the} is the thermal velocity of electrons. The physical properties of the plasma must be reproduced during the simulation.

3. Code used for simulation

The digital code used in this work is KEMPO 1D 'Kyoto University's Electromagnetic Particle Code' [12].

3.1. Methodology used to solve the basic equations

As we said previously, the basic equations used are the equation of movement (2-4) and Maxwell equations (5-8) given earlier.

By writing $F = q (E + v \times B)$ and using the finite difference method, the momentum equations can be written as follows:

$$(18) \quad \frac{x^{t+\Delta t} - x^t}{\Delta t} = v^{t+\Delta t/2}$$

$$(19) \quad m \frac{v^{t+\Delta t/2} - v^{t-\Delta t/2}}{\Delta t} = F^t$$

where the superscript index represents the temporal discretization of the equations. Figure (8) illustrates the temporal evolution of the position and velocity of each particle (equations (18) and (19)), as well as the temporal centering of commonly leap-frog used method. We simply replace two first order differential equations with two finite difference. The method used advances v^t and x^t towards $v^{t+\Delta t}$ and $x^{t+\Delta t}$. We can note that v and x are late by $t/2$.

The particles advance from position x using velocity v_x . At each temporal step Δt , the position of the particles moves forward twice, each by a step $\Delta t / 2$, as indicated below:

$$(20) \quad x^{t+\Delta t/2} = x^t + v_x^{t+\Delta t/2} \frac{\Delta t}{2}$$

$$(21) \quad x^{t+\Delta t} = x^{t+\Delta t/2} + v_x^{t+\Delta t/2} \frac{\Delta t}{2}$$

The speed of the particles is obtained by integrating the equation of motion (4) which, by the finite difference method, becomes:

$$(22) \quad \frac{v^{t+\Delta t/2} - v^{t-\Delta t/2}}{\Delta t} = \frac{q_s}{m_s} \left(E^t + \frac{v^{t+\Delta t/2} + v^{t-\Delta t/2}}{2} \times B^t \right)$$

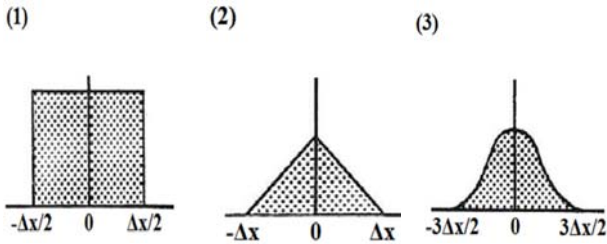


Fig.6. Super-particle shape : (1) square shape, (2) triangular shape, (3) gaussian shape

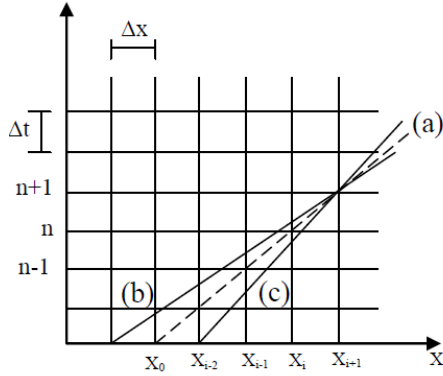


Fig.7. Geometric diagram of the CFL condition : (a) $\Delta x = c\Delta t$, (b) $\Delta x > c\Delta t$, (c) $\Delta x < c\Delta t$

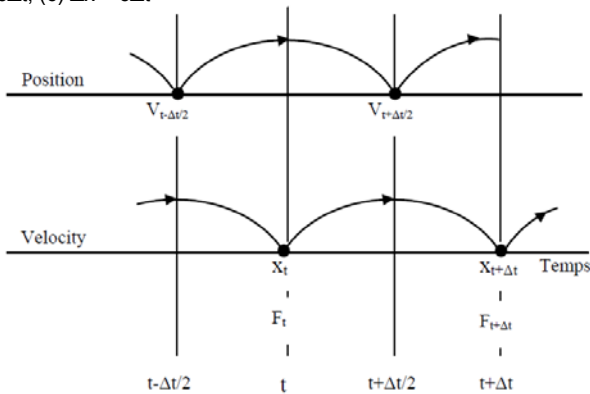


Fig.8. Diagram of the leap-frog integration method, showing the force F centered in time.

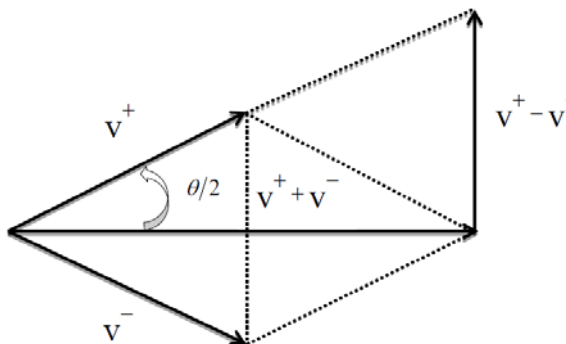


Fig.9. Vector relation for the Buneman-Boris method.

We introduce new variables v^- and v^+ in the form:

$$v^- = v^{t-\Delta t/2} + \frac{q_s}{m_s} E^t \frac{\Delta t}{2} \quad (23)$$

$$v^+ = v^{t+\Delta t/2} - \frac{q_s}{m_s} E^t \frac{\Delta t}{2} \quad (24)$$

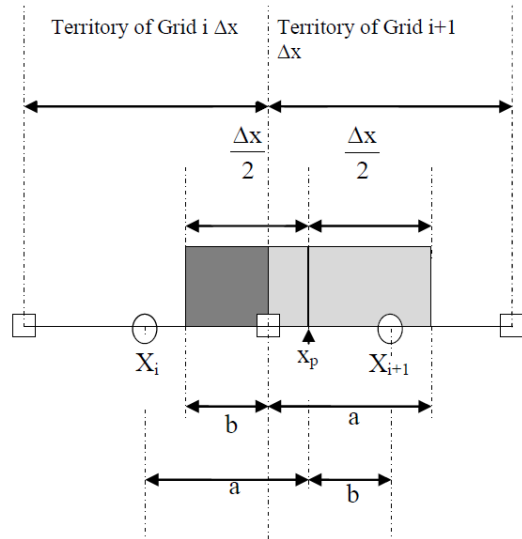


Fig.10. Area distribution method in the calculation of charge density

By replacing equations (23) and (24) in equation (22), we obtain:

$$\frac{v^+ - v^-}{\Delta t} = \frac{1}{2} \frac{q_s}{m_s} (v^+ + v^-) \times B^t \quad (25)$$

By applying the dot product in equation (25) with $(v^+ + v^-)$, we will obtain:

$$\frac{(v^+)^2 - (v^-)^2}{\Delta t} = 0 \quad (26)$$

The term to the right of equation (25) becomes null in equation (26). Indeed, the vector obtained in the cross product is perpendicular to the two vectors, the dot product

of this new vector with one or the other will therefore be null. We, therefore, notice that the term magnetic force is only responsible for varying the direction of particles motion, without changing the amplitude of the velocity. From equation (26), we have:

$$(v^+)^2 = (v^-)^2 \quad (27)$$

Figure 9 shows that equation (25) only represents a rotation with the angle θ given by:

$$\theta = -2 \tan^{-1} \left(\frac{\Delta t}{2} \frac{q_s}{m_s} B^t \right) \quad (28)$$

The particle velocity is obtained by following the four steps described below, this procedure is called the Buneman-Boris method [11]:

$$v^- = v^{t-\Delta t/2} + (q/m)_s E^t \frac{\Delta t}{2} \quad (29)$$

$$v^o = v^- + v^- \times (q/m)_s B^t \frac{\Delta t}{2} \quad (30)$$

$$v^+ = v^- + \frac{2}{1 + \left((q/m)_s B^t \frac{\Delta t}{2} \right)^2} v^o \times B^t \frac{\Delta t}{2} \quad (31)$$

$$v^{t+\Delta t/2} = v^+ + (q/m)_s E^t \frac{\Delta t}{2} \quad (32)$$

where E_t and B_t are the electric and magnetic fields linearly interpolated from the values obtained at the points of the grid. The quantity $(q/m)_s$ is the mass charge ratio of types s , and v , E and B are vectorial quantities. The components of the electric field $E \equiv (E_x, E_y, E_z)$ and of the magnetic fields $B \equiv (B_x, B_y, B_z)$ are only obtained at the discrete points of a spatial grid, from the charge density ρ and from the current density J defined at these same points of the grid. These densities are obtained from the speeds and positions of the particles, namely equations (7) and (8). By adopting a one-dimensional system along the x -axis, the electric field E_x need to meet the initial condition given by Poisson's equation [10] and Gauss' equation:

$$(33) \quad \frac{\partial E_x}{\partial x} = \frac{\rho}{\epsilon_0}$$

Poisson's equation is solved only as an initial condition of the system, this condition being automatically fulfilled if equations (7) and (8) are correctly solved in time; the current density J must meet the continuity equation and the magnetic field B_x must meet the initial condition:

$$(34) \quad \frac{\partial B_x}{\partial x} = 0$$

This condition guarantees that B_x is constant in space and time, because we only consider the one-dimensional case and we do not have the terms of B_x in Maxwell's equations (7) and (8). The current density J and the charge density ρ are obtained from the equation of motion of the particles. The electric field is calculated by integrating equation (35):

$$(35) \quad \frac{\partial E}{\partial t} = c^2 \nabla \times B - \mu_0 c^2 J$$

which for a one-dimensional system can be discretized by the following equations:

$$(36) \quad \frac{E_{x, i+1/2}^{t+\Delta t} - E_{x, i+1/2}^t}{\Delta t} = -\frac{1}{\epsilon_0} J_{x, i+1/2}^{t+\Delta t/2}$$

$$(37) \quad \frac{E_{y, i+1}^{t+\Delta t} - E_{y, i+1}^t}{\Delta t} = -c^2 \frac{B_{z, i+1/2}^{t+\Delta t/2} - B_{z, i-1/2}^{t+\Delta t/2}}{\Delta x} - \frac{1}{\epsilon_0} J_{y, i+1}^{t+\Delta t/2}$$

$$(38) \quad \frac{E_{z, i+1/2}^{t+\Delta t} - E_{z, i+1/2}^t}{\Delta t} = c^2 \frac{B_{y, i+1}^{t+\Delta t/2} - B_{y, i}^{t+\Delta t/2}}{\Delta x} - \frac{1}{\epsilon_0} J_{z, i+1/2}^{t+\Delta t/2}$$

The magnetic field is obtained by integrating equation (7). The equation in question is discretized with the following expressions:

$$(39) \quad \frac{B_{y, i}^{t+\Delta t/2} - B_{y, i}^{t-\Delta t/2}}{\Delta t} = \frac{E_{z, i+1/2}^{t+\Delta t} - E_{z, i-1/2}^{t+\Delta t}}{\Delta x}$$

$$(40) \quad \frac{B_{z, i+1/2}^{t+\Delta t/2} - B_{z, i+1/2}^{t-\Delta t/2}}{\Delta t} = -\frac{E_{y, i+1}^{t+\Delta t} - E_{y, i}^{t+\Delta t}}{\Delta x}$$

The charge density is calculated from the super particles, considered as square, as shown in figure (10). A super particles at position x_p has a $q/\Delta x$ charge distribution in the range $x_p - \Delta x/2 < x_p < x_p + \Delta x/2$. Besides, each point of the grid in X_j has an area covering a range $X_j - \Delta x/2 < X_j < X_j + \Delta x/2$. In this way, the charge of super particles q is divided into adjacent grid points, in proportion to the area shared by the grid points. Numerically, we write $q(x_p - X_j)/\Delta x$ denoted by $\rho(X_{j+1})$ and $q(X_{j+1} - x_p)/\Delta x$ indicated by $\rho(X_j)$.

The current density is obtained from the continuity equation:

$$(41) \quad \frac{\partial \rho}{\partial t} + \Delta \cdot J = 0$$

The current density has only one component along the Ox axis and discretized takes the following form:

$$(42) \quad \rho_i^{t+\Delta t} - \rho_i^t = -\left(J_{i+1/2}^{t+\Delta t} - J_{i-1/2}^{t+\Delta t}\right) \frac{\Delta t}{\Delta x}$$

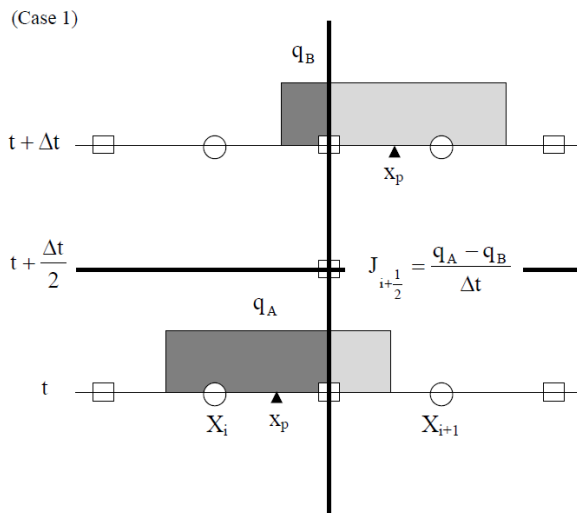


Fig.11. Charge conservation method for calculating current density when $x_p(t)$ and $x_p(t + \Delta t)$ are at the same point on the grid. In the figure q_A and q_B are defined in equation (45).

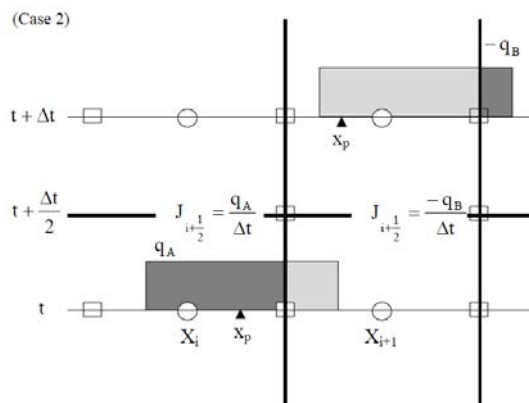


Fig.12. Charge conservation method for calculating current density when $x_p(t)$ and $x_p(t+\Delta t)$ are at different grid points. q_A and q_B are defined in (45).

Similar to the calculation of the charge density, the current density $J_x^{t+\Delta t/2}$ is obtained by satisfying equation (42). We can assume two situations since the particle does not move by more than one grid spacing Δx in a time interval Δt , i.e.:

$$(43) \quad x_p(t + \Delta t) - x_p(t) \leq \Delta x$$

where x_p is the particle position of at time t . The first case is represented in figure (11); $x_p(t)$ and $x_p(t + \Delta t)$ are both found at the same point on the grid, X_i and X_{i+1} . The second case is illustrated in figure (12), in which case $x_p(t)$ and $x_p(t + \Delta t)$ are located at different grid points. In the first case, the current density $J_{i+1/2}$ to $X_{i+1/2}$ is obtained by calculating the charge quantity passing at point $X_{i+1/2}$ at the time interval Δt :

$$(44) \quad J_{i+1/2} = \frac{q_A - q_B}{\Delta t}$$

where q_A and q_B are given by:

$$(45) \quad q_A = q \frac{X_i - x_p(t)}{\Delta x}, \quad q_B = q \frac{X_i - x_p(t + \Delta t)}{\Delta x}$$

In the second case, the particles motion contributes to the current at the points $X_{i+1/2}$ and $X_{i+3/2}$ with the two relations:

$$(46) \quad J_{i+1/2} = \frac{q_A}{\Delta t}, \quad J_{i+3/2} = -\frac{q_B}{\Delta t}$$

In figures 11 and 12, we consider the positive velocities of the particles, for a negative velocity it is necessary to multiply the right side of equations (44) and (46) by (-1).

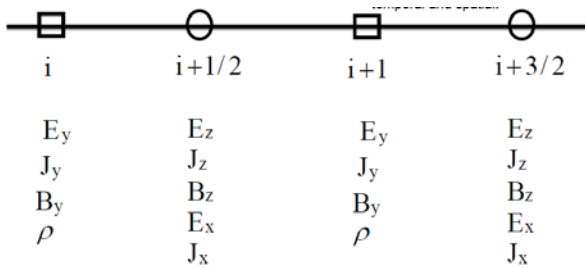


Fig.13. Spatial grid used in the KEMPO 1D code, to calculate the fields, density and current density of particles.

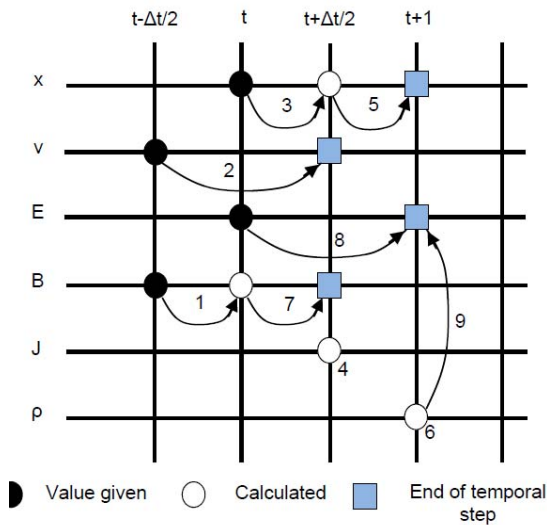


Fig.14. Evolution of the time step used in the KEMPO code to calculate the quantities of interest in the simulation.

3.2. Space grid

In the KEMPO simulation code, two grids are defined, temporal and spatial

For the spatial grid, position j on the grid is defined by the integer $j \Delta x$, ($j = 1, 2, 3, \dots, N_x$), and another position $j + 1/2$ is also defined on the grid so that the next intermediate point in the grid is given by $(j + 1/2) \Delta x$, ($j = 1, 2, 3, \dots, N_x$). This definition facilitates space-centered finite difference interpolation for the spatial derivatives of Maxwell equations.

In the code, the components E_y , B_y , J_y and ρ are defined on the j -th positions of the spatial grid, $j \Delta x$ ($j = 1, 2, 3, \dots, N_x$),

while the components E_z , B_z , J_x , J_z are defined on the $(j + 1/2)$ -th positions of the spatial grid, $(j + 1/2) \Delta x$, ($j = 1, 2, 3, \dots, N_x$), where Δx is the spacing between points on the spatial grid. Figure (13) shows the calculation diagram of the density, the components of the electromagnetic fields and the current density of the particles in the spatial grid.

Squares mark integer points and circles represent intermediate points of the spatial grid.

3.3. Time grid

As for the spatial grid, the temporal evolution is made by calculating the quantities in points and half-points of the temporal grid.

The integer points of the time grid are determined by t and the intermediate points by $(n + 1/2) \Delta t$. The electric field E and the magnetic field B are calculated by the leap method where E is calculated in integer time intervals t and B is calculated in intermediate time intervals $(n + 1/2) \Delta t$. However, the progress of Δt on the magnetic field takes place in two steps of $\Delta t/2$; its value is used to advance the position of the particles (calculated in integer multiples of Δt) [12].

The x position of the particles is also calculated at integer points of the time grid, while velocity v is obtained at intermediate points of the time grid by the frog-leap method. As for the fields, the position is advanced twice with half a time step ($\Delta t/2$) to obtain the intermediate value and calculate J at an intermediate point of the time grid. The current density is calculated from the position and velocity of the particles.

The charge density is calculated along the whole time intervals and is used to obtain the electric field. This process is illustrated in figure (14) and repeated as many times as necessary to obtain the results of the simulation.

3.4. Standardization and unity system

To perform the simulations, it is not necessary to define a real unit system such as CGS or SI. The important thing is to define the ratios between the quantities of the system used, that is to say the ratio between the magnetic field of the wave and the magnetostatic field or the ratio between the kinetic energy of the ambient plasma and the total system energy, etc. During the simulations, the physical quantities are standardized, which makes the basic parameters of the system become dimensionless. However, the selection of basic parameters may vary depending on the physical model adopted. Develop simulation code applicable to various Physics problems and with a large system of variables taking into account a set of basic parameters to obtain the fundamental equations. These parameters are:

- a. Angular frequency (plasma, cyclotron, wave frequency, etc.) ω_{pi} , Ω_{c1} , ω ;
- b. System length L_x ;
- c. Load to mass ratio $(q/m)_i$;
- d. Number of super particles in the N_i system ;

where the subscript i denotes the i th type of particles. The cyclotron frequency is specifically defined for type 1 and is related to the intensity of the ambient magnetic field. The values of these four quantities are given in an arbitrary manner, except that the ratios between the quantities in the same unit system, ω_{pi}/Ω_{c1} , $\Delta x/L_x$ or $(q/m)_2/(q/m)_1$, have kept real physical quantities. The number of super particles has no relation to the numerical density of the real plasma particles and N_1 and N_2 are independent of each other.

The basic equations are written in such a way as to be identical to the equations of motion and of Maxwell in the international system. The values of electrical permittivity ϵ_0

and magnetic permeability μ_0 can be defined arbitrarily, provided that they satisfy the equation (9).

By adopting a one-dimensional system along the x-axis, the electric field E_x needs to meet the initial condition given by Poisson's equation [14] and Gauss' equation:

$$(47) \quad \frac{\partial E_x}{\partial x} = \frac{\rho}{\varepsilon_0}$$

The physical quantities are calculated by following the relationships obtained from the basic equations. The cyclotron frequency for types 1 and the plasma frequency for types i are given by:

$$(48) \quad \Omega_{c1} = \frac{q_1}{m_1} B_0, \quad w_{pi} = \sqrt{\frac{n_i q_i^2}{m_i \varepsilon_0}}$$

where n_i is the particles density of type i which can be obtained by:

$$(49) \quad n_i = \frac{N_i}{L_x}$$

From equations (48) and (49), we obtain the following physical quantities:

- Particles charge:

$$(50) \quad q_i = \frac{\varepsilon_0 L_x w_{pi}^2}{N_i (q/m)_i}$$

- Particles mass:

$$(51) \quad m_i = \frac{\varepsilon_0 L_x w_{pi}^2}{N_i (q/m)_i^2}$$

- Magnetostatic field :

$$(52) \quad B_0 = \frac{\Omega_{c1}}{(q/m)_1}$$

We note that the mass m_i and the charge q_i do not matter much in the physical calculation system. To perform the simulations, the most important parameters, physically speaking, are mass density n_i , m_i and charge density $n_i q_i$, given by:

$$(53) \quad n_i m_i = \frac{\varepsilon_0 w_{pi}^2}{(q/m)_i^2}, \quad n_i q_i = \frac{\varepsilon_0 w_{pi}^2}{(q/m)_i}$$

The values of w_{pi} and $(q/m)_i$ for the different types must be taken into account during the simulations. Once the spatiotemporal grids are defined, as well as the system of equations used in the simulation with the appropriate boundary conditions, particle simulations can be used to study a series of plasma physics phenomena, as we will see later.

4. Results and discussion

Particle simulations allow us to obtain a great deal of information on the physical behavior of plasmas in space and in laboratories. In what follows, we present some results obtained with particle simulations for classical phenomena of plasma physics which occur in laboratory and space plasmas. We will also try to illustrate the importance of defining the parameters used to ensure the correct resolution of the problem. In the first example, we present the result of the simulation of an electromagnetic

oscillation in plasma in order to visualize the importance of ensuring that the CFL condition is met throughout the simulations. Table (1) shows the parameters used in the simulation, where q/m is the mass charge ratio, PCH is the angle between wave number k and field B , v_{pa} and v_{pe} are the parallel and perpendicular thermal speeds of particles, NX, NTIME and NP represent the number of points of the spatial grid, the number of temporal intervals and the number of particles of a given type ($NS = 1$) involved in the simulation.

The other parameters have been defined previously.

Table 1. Plasma parameters for figures simulation (15-16).

Setting	Value	Setting	Value
Δx	1,0	NX	128
Δt	0,1	NTIME	4096
c	8,0	NP	1024
w_{pe}	1,0	PCH	0
v_{pe}	0,5	v_{pa}	0,5
Ω_c	-1,0	q/m	-1,0

In figure (15), for the left curves, the CFL condition is satisfied ($\Delta x > v_{max} \Delta t$) and the parameters used are the same as in table (1). We can see that during the simulation, the total energy of the system (T) (sum of electrical energy (E) and kinetic energy (K)) remains constant.

Thus, we notice that electric field E_x is almost stable and revolves around zero. In case (b), we consider ($\Delta x \approx v_{max} \Delta t$). In this case, we can perceive a variation of the total energy of the system (variation of electric energy E due to the instability of the electric field E_x , in addition to the variation of the kinetic energy K due to the movement of a large number of particles).

This variation is related to numerical fluctuations which themselves are related to the number of particles per point in the grid since we have not introduced any source term in the system. The total energy variation results from numerical instabilities.

For the right-hand curves, we cannot fully rely on the results of the simulations because numerical instabilities can modify the physical behavior of the system.

Figure (16) shows another example of a simulation in which we show the dispersion ratios of a magnetized plasma and the phase space of the particles. In this example, we consider the parameters of table (1) with the following different parameters, $NX = 256$, $NTIME = 1024$, $w_{pe} = 2.0$ and $v_{pa} = v_{pe} = 1.0$. We consider a propagation parallel to the external magnetic field $k \parallel B_0$. The mode at the plasma frequency $w_{pe} = 2.0$ corresponds to Langmuir waves: waves in R mode and L mode whose phase speeds approach the speed of light and a wave in whistler mode whose frequency is lower than the frequency of the electronic cyclotron.

The dispersion relation of a polarized wave in right-hand mode (R) in a circular manner is given by: and the left-handed polarized mode in a circular manner (L) is defined by:

$$(54) \quad \frac{k^2 c^2}{w^2} = 1 - \frac{w_{pe}^2}{w(w - \Omega_c)}$$

and the left-handed polarized mode in a circular manner (L) is defined by:

$$(55) \quad \frac{k^2 c^2}{w^2} = 1 - \frac{w_{pe}^2}{w(w + \Omega_c)}$$

We have also drawn phase diagrams of particles in the x - V_x space in the right-hand panel of figure (16), but the ω - k diagrams do not appear until after the end of the analysis. It is also noted that the dispersion relation of the light mode with its phase speed close to the speed of light is distorted in the high wave number range close to wave number $k_{max} = \pi / \Delta x$. This is due to the centered difference pattern expressed in (16).

We now introduce two different groups of electrons, in addition to the ions that are supposed to form a neutralizing background, as in the previous tests. The two groups of electrons have different drift speeds in the direction parallel to the static magnetic field. If the thermal speeds of the electrons are much smaller than the relative drift speed between the two groups of electrons, a strong electrostatic instability occurs. The instability growth rate is so large that it can be demonstrated despite large thermal fluctuations. The parameters used are shown in table (2), where v_D (a) and v_D (b) are the drift rates for types (a) and (b) respectively.

Table 2. Plasma parameters for figures simulation (17-20)

Setting	Value	Setting	Value
Δx	1,0	NX	64
Δt	0,04		
c	20,0	NS	2
Ω_c	-1,0	q/m	-1,0
w_{pe}	2,0	v_{pe}	1,0
v_{pa}	1,0	PCH	0,0
NS (a)	électrons	NS (b)	électrons
v_D (a)	0,0	v_D (b)	10,0

We first study the growth and saturation of the two-flux instability NP (a) = NP (b) = 256 with $NTIME = 128$ and 256 (see figures (17) and (18)). We note that a coherent electrostatic potential develops to trap most of the electrons ($NTIME = 128$) (figure (17)). Electrons undergo a nonlinear oscillation in vortex-forming potentials.

The instability is saturated because of the mixing of the two electron flows ($NTIME = 256$) (figure (18)). Second, we try a longer time interval with $NTIME = 2048$, while keeping the same number of particles NP (a) = NP (b) = 256. We note that the phase mixing continues with the dissipation of trapping potentials (figure (19)).

Third, we increase the number of particles in order to reduce the thermal noise level by setting NP (a) = NP (b) = 4096 and run the code with $NTIME = 2048$.

We find the formation of very stable potential structures by the coalescence of smaller potentials, as shown in figure (20). These potential structures are called electron holes, as found in the space-phase velocity diagram in the upper left-hand panel, or electrostatic solitary waves (ESW), as

For the third simulation series, we study two electron beams of the same density and with reversed fluxes strongly interacting and thus forming non-linear electrostatic potentials which can then merge to form an ESW. Importantly, in this simple description, ion dynamics is overlooked as a fixed neutralizing background.

When incorporating mobile ions into our simulations, we have noted that ion dynamics plays an important role in the formation of ESWs. The electron beams and an ion beam whose densities are n_1 , n_2 and n_i respectively: ($n_1 + n_2 = n_i$).

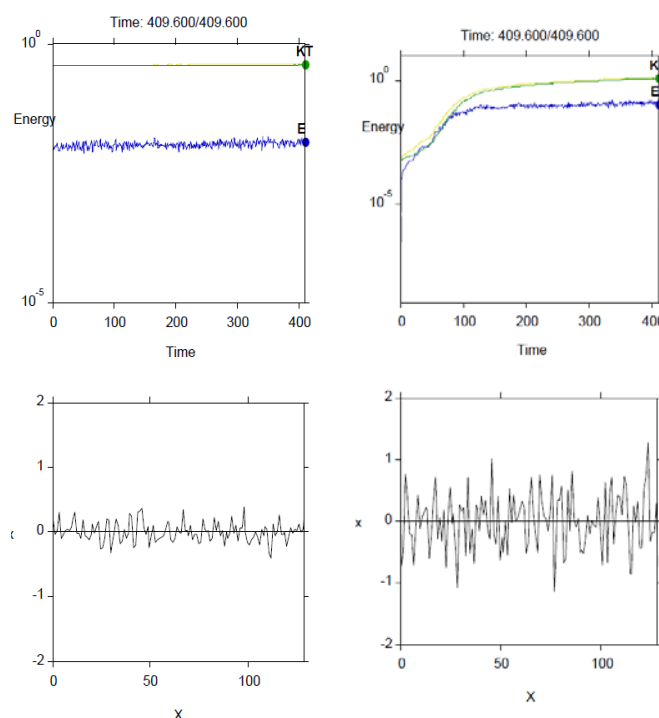


Fig.15. Simulation pour vérifier la condition CFL. Figures de gauche : stable. Droite : instable.

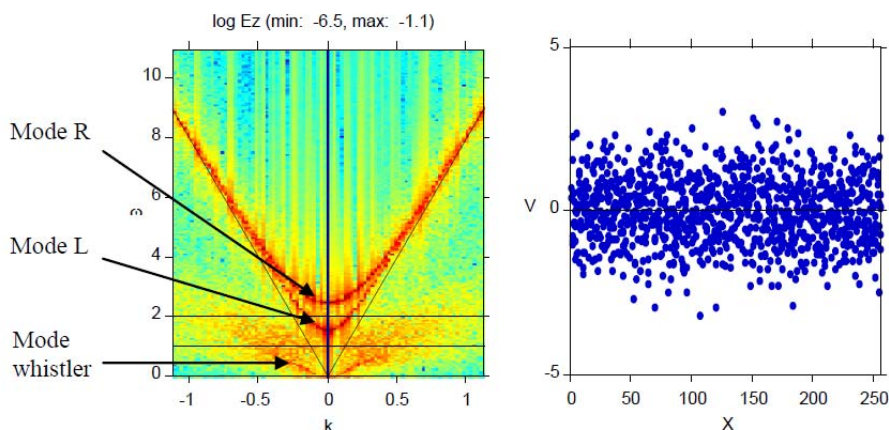


Fig.16. Dispersion relationship for high frequency modes (R), low frequency (L) and whistler.

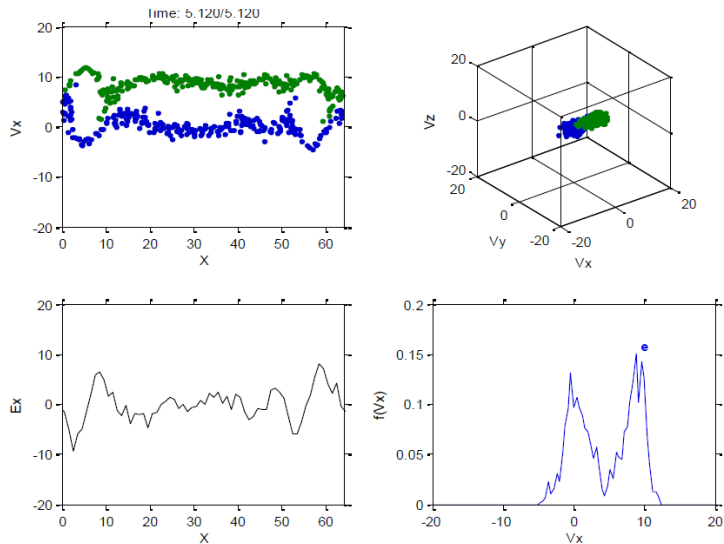


Fig.17. Simulation of the instability of two electron beams (NP(a) = NP(b) = 256, NTIME = 128)

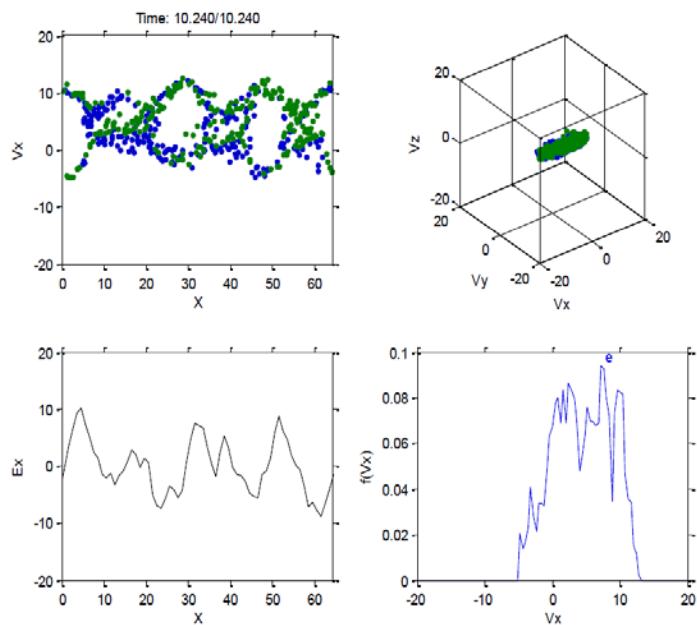


Fig.18. Simulation of the instability of two electron beams (NP(a) = NP(b) = 256, NTIME = 256)

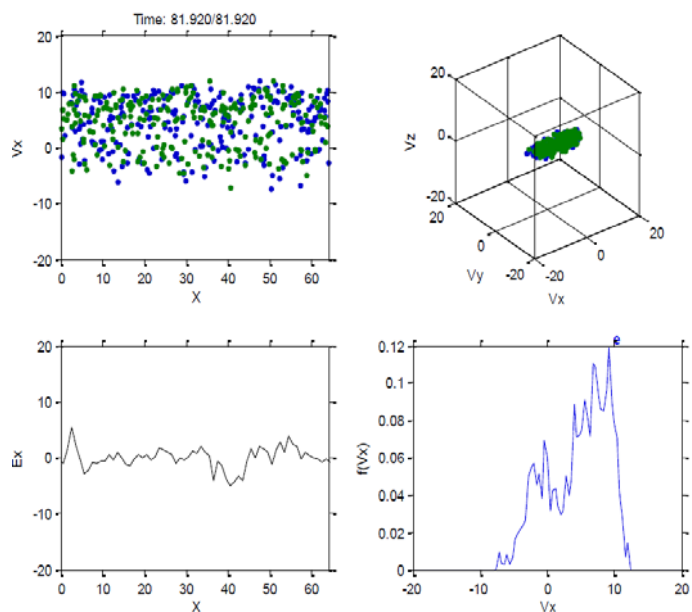


Fig.19. Simulation of the instability of two electron beams (NP(a) = NP(b) = 256, NTIME = 2048)

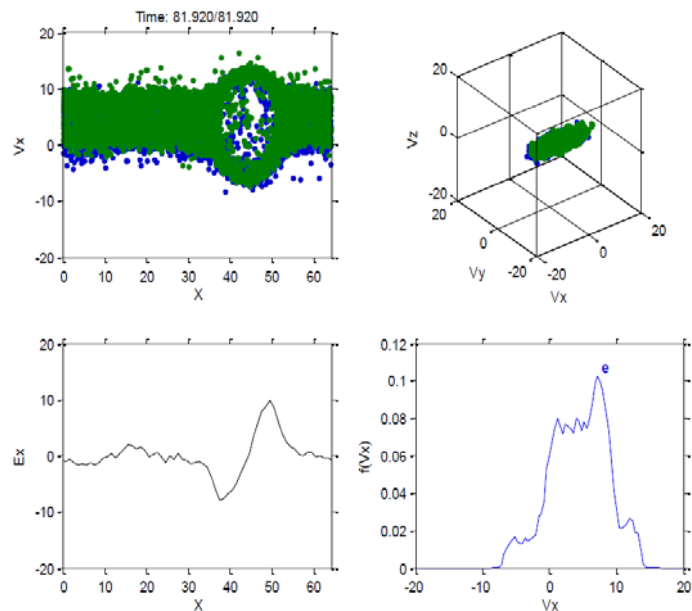
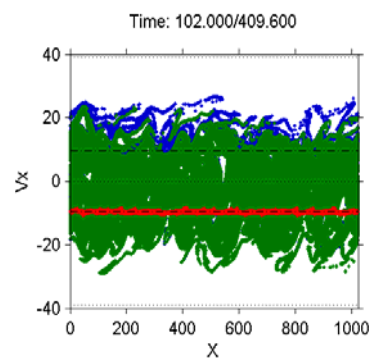
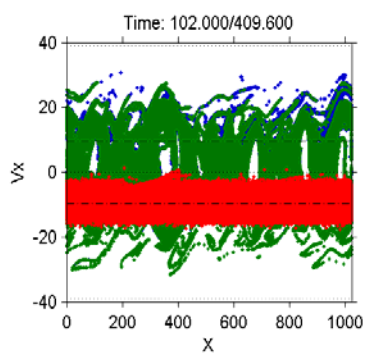
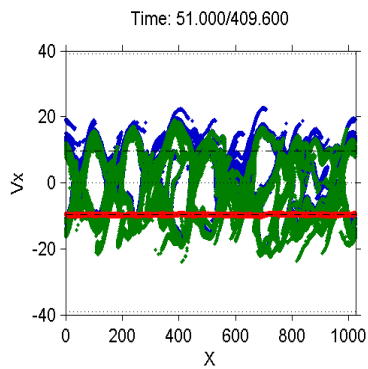
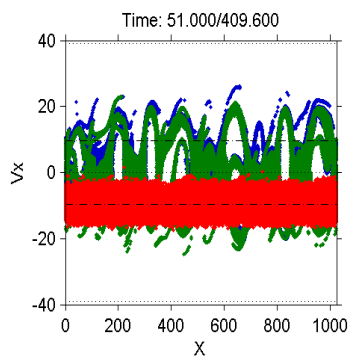
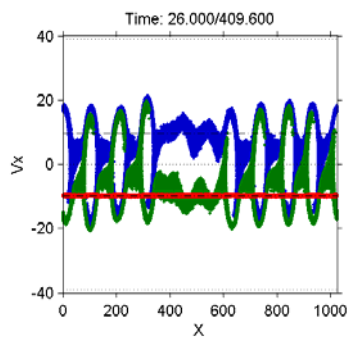
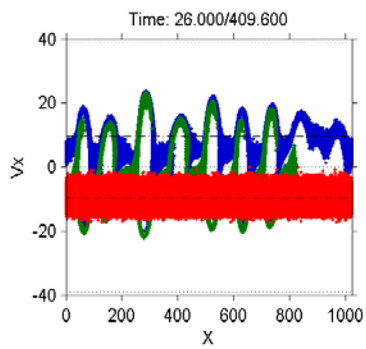


Fig.20. Simulation of the instability of two electron beams (NP(a) = NP(b) = 4096, NTIME = 2048)

(a) $v_i/v_D = 0.1$

(b) $v_i/v_D = 0.005$



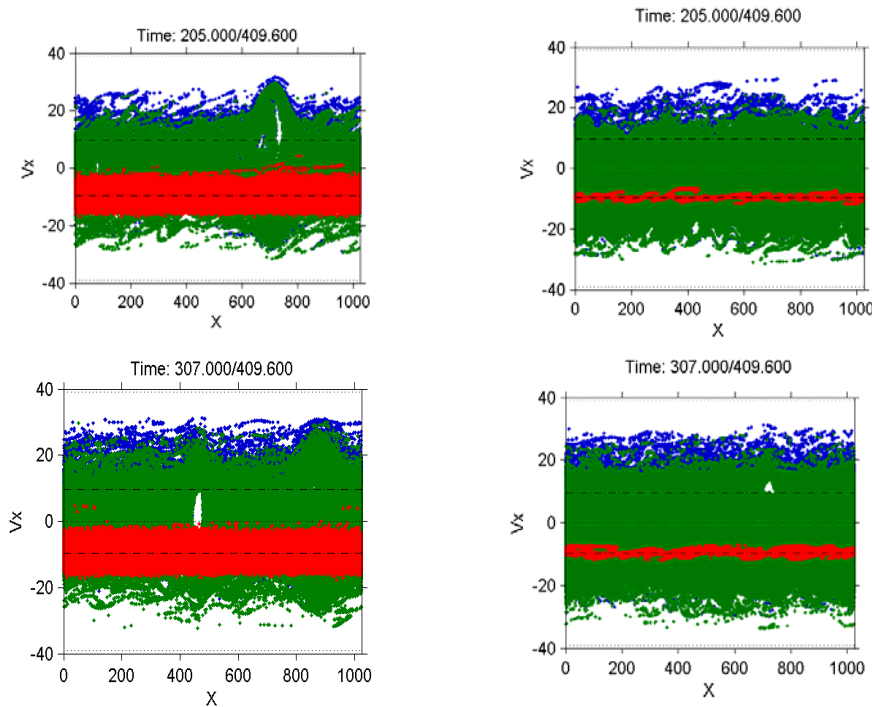


Fig.21. Particules in $v_x - x$ at $t = 26, 51, 102, 205$ et 307 with $R = 0,5$

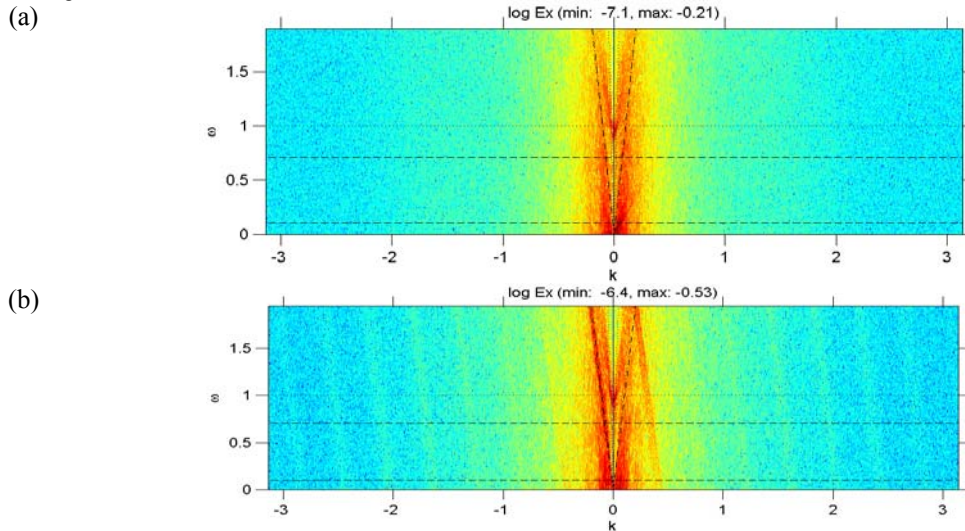


Fig.22. Frequency spectra (w) and wave number (k) de E_x for the time $t = 409,6$ with $R = 0.5$ and (a) $v_i/v_D = 0.1$, (b) $v_i/v_D = 0.005$

One electron beam (of density n_1) assumes a drift velocity $V_D/2$, while the other electron beam with n_2 and the ion beam with n_i have drift velocities $-V_D/2$.

We also assume that the beam velocity distributions are Maxwellian but shifted by the above drift velocities. The thermal velocities are v_e for the two electron beams and v_i for the ion beam, respectively. In the following simulations, we vary the thermal speed of the v_i ions. We define density ratio $R = n_1 / n_i$ as a parameter.

The other parameters are listed in table (3).

We perform two tests with different initial thermal velocities v_i ($v_i / v_D = 0,1$ et $0,005$) and the same density ratio $R = 0.5$. The evolution of the instability is illustrated by the phase diagrams of the particles in the $x-V_x$ space in figure (21). At $t = 26 w_{pe}^{-1}$, we note wave excitation around mode 10 (10 spatial wave cycles in the system), which is equivalent to $k = 12 w_{pe}/V_D$, and we see no significant difference between the two cases (a) and (b). However, at $t = 51 w_{pe}^{-1}$, we find that the number of trapped electron

vortices coalesces down in the left panel ($v_i/v_D = 0.1$), while the right panel ($v_i/v_D = 0.005$) displays a slightly disordered vortex structure. Later, at $t = 102, 205$ and 307 , we observe the formation of larger vortices corresponding to ESWs by the coalescence of smaller vortices on the left, while the vortices seem to disappear in the right panel.

Figure (22) represents the $w - k$ spectra obtained by the Fourier transformation of electric fields in space and time for the period $t = 1,6 w_{pe}^{-1} \sim 409,6 w_{pe}^{-1}$. Panels (a) and (b) correspond respectively to the cases (a) and (b) of figure (21).

In panel (a), the wavenumber spectra are limited in the region of $k = 0 \sim 1.2 w_{pe}/V_D$. From the dispersion slope, we can talk of the final ESW movement with a speed of $0,26 v_D$. In figure (b) we find two dominant modes covering a wider range of wavenumber $k < 2.4 w_{pe}/V_D$.

These modes represent the acoustic waves of the ions in the ion beam frame and have phase speeds $-v_D/2 \pm v_s$, where v_s is the speed of sound of ions.

In both cases, the electrons are thermalized in the speed range between the drift speeds $\pm v_D/2$ and the strong nonlinear trapping of all the electron beams, as shown in Figure (21).

Table 3. Plasma parameters used for the simulation of the figure (21)

Setting	Value	Setting	Value
Δx	1,0	NX	1024
Δt	0,025	NTIME	16384
v_D	10	m_e/m_i	0.01
w_{pe}	1,0	w_{pi}	0,1
v_e	1,0	v_i	1,0 - 0,05
NP (e)	524288	NP (i)	1048576

We can thus estimate the thermal velocity of electrons v_e in the nonlinear stage in $\sim v_D/2$. If v_i is negligible, ionic sound waves can propagate without Landau ion damping at the phase velocity v_s given by:

$$v_s \approx \sqrt{m_e/m_i} v_D/2$$

Since we assumed that the parameters which give $v_s/v_D = 0.05$ at the nonlinear stage of electron trapping, $v_i \ll v_s$ is satisfied for the case of Panel (b). Therefore, the initial electrostatic waves due to the two-flux instability are converted to ionic acoustic waves at higher wavenumbers. However, in the case of panel (a) ($v_i/v_D = 0.1$), $v_i > v_s$, where the ionic sound waves are strongly damped. Since there are no other modes in which electrostatic waves can decay, the coalescence of trapped electrons leads to the formation of ESW.

5. Conclusion

In this article, we present some characteristics of particle simulations applied to plasma simulation. We identify a few criteria required to perform computer simulations and the steps to follow for the temporal and spatial evolution of a set of particles of a magnetized plasma.

We introduce one dimensional computer simulation in plasma physics. We also present some characteristics of particle simulations applied to plasma simulation. We show some criteria necessary to perform computer simulations and the steps to follow for the temporal and spatial evolution of a set of particles of magnetized plasma.

We underline the care that must be taken in the initial conditions of the simulation to avoid numerical instabilities which can lead to a corrupt physical behavior of the system. In the case where external sources are not included, the digital instabilities are characterized by the variation of the total energy (T) of the system.

Other diagnoses can be obtained by computer simulations depending on the type of phenomena under study. We also simulated two electron beams of the same density and with reversed fluxes strongly interacting, thus forming nonlinear electrostatic potentials which can then merge to form an ESW. Importantly, in this simple description, ion dynamics has been overlooked as a fixed neutralizing background. We incorporated mobile ions into our simulations and found that ion dynamics plays an important role in the formation of ESWs.

Computer simulations are not, and probably never will be, the solution to all the physical problems, but they are a powerful tool that can help researchers solve many unanswered Physics problems, especially those related to non-linear and time dependent systems.

At this day, more realistic simulations are made and constantly upgraded. Simulation are not limited to one dimension, interaction between particles is not only through field but also by direct collisions. To speed up simulations and capability to simulate more particles, program are adjusted to run simultaneously on several computer processors and the simulation performance is done by using new numerical methods.

Computer simulations are not, and probably never will be, the solution to all the physical problems, but they are a powerful tool that can help researchers solve many unanswered Physics problems, especially those related to non-linear and time dependent systems.

Authors

Housseyn Tazrout (Dr) is doctor at University Science of technology of Oran, Algeria.

Aicha Flitti (Pr) is currently a Professor at University of Sciences and Technology of Oran, Algeria. E-mail: afaouicha90@gmail.com

REFERENCES

- G. Lapenta, Introduction to particle in cell, Notes provided <https://github.com/CmPA/iPic3D/wiki/School-in-Les-Houches>.
- F.F. Chen, Introduction to plasma physics and controlled fusion, Plenum Press, New York, 1984, volume 1.
- C. K. Birdsall, A.B. Langdon, Plasma physics via computer science, Taylor and Francis LTD, October 2004
- M. V. Alves, Kinetic simulation in plasmas: A general view and some applications, INP-7171-PRE/3096, 1999.
- Yu. N. Grigoryev, V.A. Vshykov and M.P. Fedoruk, Numerical particle in cell methods, theory and applications, Utrecht Boston 2002.
- M E Dieckmann, The particle in cell simulation: concepts and limitation, Summer College on Plasma Physics, Summer College on Plasma Physics, 30 July -24 August 2007, The Abdussalam Center of Physics.
- M. Grech, The particle in cell (PIC) simulation of plasmas, LULI CNRS, Les Houches, Mai 2019.
- J.M. Dawson, Reviews of Modern Physics, 403, 1983.
- D. Potter, Computational Physics, John Wiley and Sons, 1973.
- H. Matsumoto and T. Sato Computer Simulation of Space Plasmas, Terra Scientific Publishing Company, Tokyo, 1985.
- C.K. Birdsall and A.B. Langdon, Plasma Physics via Computer Simulation, Institute of Physics Publishing, London, 1991.
- H. Matsumoto and Y. Omura Computer Space Plasma Physics: Simulation Techniques and Software, Terra scientific publishing company, Tokyo, 1993.
- A.B. Langdon and C.K. Birdsall, Physics of Fluids 2115, 1970.
- H. Okuda and J.M. Dawson, Physics of Fluids, 408, 1973.
- A.O. Fortuna, Técnicas Computacionais Para Dinâmica dos Fluidos (Editora da Universidade de São Paulo, São Paulo, 2000).
- R.W. Hocney, Physics of Fluids 9 1826, 1969.
- C.K. Birdsall and D. Fuss, J. of Computational Physics, 135, 141, 1997.
- H. Okuda and C.K. Birdsall, Physics of Fluids, 2123, 1970.
- R.L. Morse and C.W. Nielson, Physics of Fluids, 2418, (1969).
- A.B. Langdon and C.K. Birdsall, Physics of Fluids 2115, (1970).